



Czech Technical University in Prague
Faculty of Nuclear Sciences and Physical Engineering
Department of Physics

CHARACTERIZATION OF MONOLITHIC DETECTORS FOR SPACE APPLICATIONS

RESEARCH TASK

Bc. Anežka Kabátová

Field of study: Experimental Nuclear and Particle Physics
Supervisor: Ing. Michal Marčíšovský, Ph.D.
Academic year: 2019

Statement of authorship

I hereby declare that I am the sole author of this research task and that I have not used any sources other than those listed in the bibliography and identified as references.

In Prague 17th September

Signature

Acknowledgement

I would like to warmly thank to my supervisor Michal Marčišovský and to my consultant Mária Marčišovská for their infinite patience, pieces of advice, comments and feedbacks, which they provided during my work.

Title:

Characterization of monolithic detectors for space applications

Author: Bc. Anežka Kabátová

Field of study: Experimental Nuclear and Particle Physics

Type of Work: Research Task

Supervisor: Ing. Michal Marčíšovský, Ph.D.

Consultant: Ing. Mária Marčíšovská, Ph.D.

Abstract: The following research task focuses on the characterization of a monolithic silicon detection chip X-CHIP-03 dedicated to imaging and dosimetric applications. It also serves the purpose of a prototype for the future generation of detectors of the space environment. Thus, this paper resolves around radiation present in the near-Earth space, effects of this radiation on electric circuits and mainly around testing of X-CHIP-03 during irradiation and dynamic temperature changes to prove the sufficiency of its capabilities. The last chapter is dedicated to the summary of the Socrat-R mission within which was X-CHIP-03 launched to the sun synchronous orbit.

Key words: semiconductor detectors, space environment, radiation damage

Contents

1	Introduction	1
2	Space environment	4
2.1	The SSO 530 orbit	5
3	Radiation damage in semiconductors	14
4	Radiation tolerance of X-CHIP-03	16
4.1	Simulations of experiments	16
4.1.1	Geant4	16
4.1.2	SRIM	17
4.2	Single event upset evaluation	18
4.2.1	Experiment in Joint Institute for Nuclear Research	18
4.2.2	Experiment in the Nuclear Physics Institute	19
4.2.3	Results	21
4.2.4	Homogeneity of bit-flip sensitivity	21
5	Characterization of X-CHIP-03 response	26
6	X-CHIP-03 in space	29
7	Conclusions	33

Acronyms

ASIC Application-specific Integrated Circuit. 21

CAPADS Center of Applied Physics and Advanced Detector Systems. 3

GCR Galactic Cosmic Rays. 4

JINR Joint Institute for Nuclear Research. 19

LET Linear Energy Transfer. 2

NPI CAS Nuclear Physics Institute of the Czech Academy of Sciences. 19

SEU Single Event Upset. 1

SoI Silicon on Insulator. 1

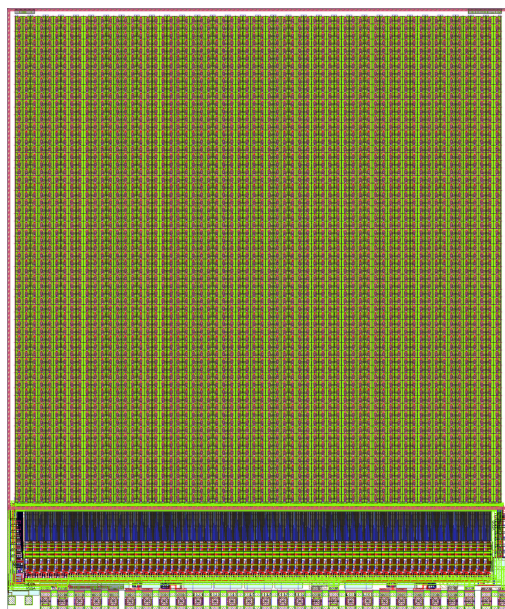
SXRM SpacePix Radiation Monitor. 17

1 Introduction

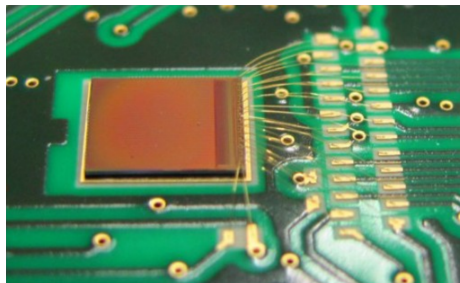
This work presents a number of experiments performed on a radiation detection device X-CHIP-03 in order to test its characteristics and improve design of the future generation of detectors. X-CHIP-03 is a monolithic silicon detection chip based on the 180 nm SoI technology which consists of square pixel cells with a $60\ \mu\text{m}$ pitch forming an array of 64×64 pixels, covering an active surface of $3.84 \times 3.84\ \text{mm}^2$. X-CHIP-03 has two operation modes – hit counting mode and ADC mode dedicated to the measurement of deposited energy in pixels [1].

Although this device can be used for a number of purposes, the result of the experiments should be directly linked to the future design improvement in order to fulfil a long-term challenge of creating a detector of cosmic radiation, SpacePix, to be used in-situ.

Among the requirements to meet such a challenging task is a sufficient single event upset (SEU) tolerance. Since devices in the cosmic environment are exposed to high radiation doses as well as encounters with heavy ions, they must be able to withstand those conditions and be thoroughly tested for them.



(a) A scheme of X-CHIP-03.



(b) X-CHIP-03 wire-bonded to PCB.



(c) SpacePix Demonstrator currently using X-CHIP-03.

Fig. 1.1. Experimental set of SpacePix Demonstrator and currently used ASIC - X-CHIP-03.

For the evaluation of SEU cross-section of X-CHIP-03, data from irradiation by protons and various ions (helium, carbon, lithium, xenon, argon, neon) were used. X-CHIP-03 was tested in several experimental facilities namely the Joint Institute for Nuclear Research in Dubna, Russia, using a cyclotron U400M [2], and the Nuclear Physics Institute of the Czech Academy of Sciences in Řež where the beam was accelerated by a tandem accelerator Tandetron [3]. The result of performed experiments is a characteristic response plot representing the dependence of the mentioned SEU cross-section on the linear energy transfer (LET) of a particle impinging on it.

Currently, X-CHIP-03 is used in SpacePix Demonstrator [4] - a battery powered standalone technology demonstrator of a pixelated monolithic radiation detector. It is providing valuable feedback of its performance, albeit at a limited dynamic range that is to be improved for the SpacePix family. In the Fig. 1.1, a scheme and a photo of the X-CHIP-03 ASIC can be found, as well as the photo of SpacePix Demonstrator.

These experiments are described in detail in Section 3.

Besides the radiation tolerance testing of X-CHIP-03, the energy calibration has been performed. The result of the calibration is crucial for the complete knowledge of characteristics of detected particles. The natural units of the detection device are the so called *ADC units* or units of analogue-to-digital converter (1 ADC unit corresponds to approximately 1 mV of peak voltage). This feature is a result of the way how the signal in the device is created. The ionising particle passing through the chip volume creates electron-hole pairs which subsequently travel to the corresponding electrodes. This movement generates a current which is dependent on the original energy of the particle through the number of created pairs. The current is then processed in the circuit and finally converted in the mentioned ADC units. To reconstruct information about the energy of the passing particle, it is necessary to investigate its relation to ADC units. This is carried out using well-known spectra of radioactive elements which can be used to assign particular spectral peaks to a certain value in ADC units.



Fig. 1.2. Left: The orbit of the Socrat satellite carrying the detection device X-CHIP-03 [5]. Right: The start of Soyuz rocket carrying the Socrat satellite from the Vostochny Cosmodrome in eastern Russia [6].

Another characteristic of the cosmic environment is the wide temperature range in which the device can operate. Therefore, the next point of interest was to investigate whether the detector response (alongside with the calibration result) is temperature dependent. In that case, special attention would have to be paid to the temperature mea-

surement during an in-situ cosmic radiation experiment in order to remove the emerged temperature bias. The results of the both experiments are described in Section 5.

The last chapter of this work is dedicated to the first in-situ experiment starting in July 2019 performed by the Center of Applied Physics and Advanced Detector Systems (CAPADS) ¹ when X-CHIP-03 and its descendant SpacePix were sent to the sun synchronous orbit by the Soyuz 2.1b/Fregat rocket (Fig. 1.2) as a component of the Socrat-R satellite built at the Lomonosov university in Moscow.

¹<http://capads.fjfi.cvut.cz/>

2 Space environment

The very broad term *space environment* includes the description of temperatures, particles of the cosmic radiation and macroscopic objects that are present in the space and possibly endanger space systems. Depending on multiple factors, effects of these collisions can be destructive for the system. Many present surveys aim to study, monitor and predict the space environment and its actual state - space weather, to protect not only people on the manned missions, expensive devices and their components, but also systems on the planet Earth that can be influenced in the case of the extreme space weather with considerable consequences such as radio blackout.

For the devices dedicated to study near-Earth space environment, the situation is specific and to some extent differs from the general space conditions. The common constituent of the space environment across the galaxy are galactic cosmic rays (GCR). GCRs originate outside our solar system in explosive events such as supernovae explosions. However, the fact that GCR particles are charged, and therefore influenced by magnetic fields, makes it very challenging to assign them to their source. The composition of GCR spectra is dominated by hydrogen (about 89%) followed by heavier elements up to uranium, although its abundance is approximately 11 order of magnitude lower than the one of the hydrogen [7]. The energy of such particles varies from 1 to 10^5 MeV but most likely reaches several hundreds MeV [8]. In the proximity of the Sun the GCR is flux modulated by its magnetic field, especially when the Sun reaches its maximum in 11-year-long cycle. This effect can be seen particularly on lower-energy particles that experience the strongest attenuation [7].

The Sun is the main contributor on the space environment near Earth. Besides influencing GCR, it is a source of particles itself. Through solar flares and coronal mass ejections (CMEs) originating in dynamic changes of magnetic field of the Sun, radiation and particles of high energies, that can have direct impact on systems on Earth, are released. When the solar flare is abnormally strong, the radiation impinging on Earth causes an extraordinary ionisation in the ionosphere. Free electrons that are created by the ionisation then collide with radio waves that lose energy by these more frequent encounters. This can result in a radio blackout. However, most of the time, solar flares do not influence Earth's systems [9].

Another important threat to technology in the near-Earth space environment are so-called radiation belts. Radiation, or Van Allen belts are dynamic regions with high population of electrons and protons. They are created and lead by the Earth magnetic field and heavily impacted by its interaction with solar wind. Electrons typically form two separate belts - the inner and the outer - extending from 1.5 to 3 and from 3 to 10 earth radii, respectively. The inner electron belt is overlapping with proton belt containing particles of energy above 10 MeV [10].

The Earth is protected from most of the high energy particles by its magnetosphere

and atmosphere. However, there are regions of near-zero magnetic field through which particles can penetrate the atmosphere. These are called *polar cusps*. They are located on the boundary between sunward and tailward lines of the magnetic field. In this region, Earth's magnetic field lines are "open" in the sense that they can directly connect to the interplanetary magnetic field lines carried by plasma. Particles that enter the atmosphere subsequently interact with its atoms creating auroras in the process of de-excitation [11]. All of these phenomena from the solar-terrestrial system account for most of the effects of the near-Earth space environment. However, there are also processes of more random nature that can easily cause the destruction of a system. One of them is induced by a comet passing in the vicinity of the Sun. Due to the solar wind, parts of the comet are freed and follow it on its orbit as meteoroids. When the path of the comet is nearby the Earth's orbit around the Sun, they can cause a meteor shower by penetrating the atmosphere. Although a direct hit by such an object would naturally cause the destruction of the affected technology, it is very unlikely to happen. The greater danger represent smaller particles that continuously impinge on the surface of the devices resulting in cracks in them. This penetration subsequently allows the corrosion by an atomic oxygen [12]. To protect the Earth from the possible encounters with natural objects and their consequences, Near-Earth Object Coordination Centre (NEOCC) was established [13]. Its mission is to map and predict trajectories of objects near Earth and put them potentially on the *risk list* to control their development. NEOCC is one of the segments of ESA's Space Situation Awareness (SSA) programme launched in 2009. The other two segments are the Space Weather and Space Surveillance and Tracking. While the objectives of the former are clear from its title, the later covers human-induced effects on the cosmic environment.

With the increasing number of experiments that have been run in the near-Earth space from the beginning of the in-situ research, another threat to the present-day experiments is represented by debris. Space debris, or the remnants of the disrupted devices, can also collide with satellites or even re-enter the atmosphere and fall on the surface of Earth [14]. ESA's Space Surveillance and Tracking Segment was set up to detect and predict the movement of space debris in orbit around Earth, issuing warnings and guidance to spacecraft operators [15].

■ 2.1 The SSO 530 orbit

To quantify properties of the specific environment that pixel detectors sent on the orbit as a part of the SOCRAT-R mission in July 2019 occupy, series of simulations were performed using the SPENVIS software [16]. After coordinates of the concrete mission are input, using user-chosen models, particle fluxes, spectra, distributions and much more can be simulated. The SOCRAT-R mission is situated in the altitude ranging from the 513 km perigee and 548 km apogee. The inclination of the satellite orbit is 97.5° which is close to the polar orbit. Currently, in 2019, the activity of the Sun is at the minimum indicating that GCR fluxes reach their maxima. Besides GCR and solar proton fluxes, Van Allen belts abundance of protons and electrons was simulated. For the latest, AP-8 and AE-8 models [17] were used.

Developed by NASA Space Science Data Coordinated Archive (NSSDC), both AP-8 and AE-8 models are widely successfully used. They are based on the data collected in 1958 and 1979 by 38 satellites. They contain omni-directional flux of particles as a

function of idealized geomagnetic dipole coordinates with a spacial coverage remaining unreachable for the recent models. However, there are reasonable doubts whether these 20-year-old models still reflect the current dynamic environment. Also, apart from the solar minimum and maximum specification, adjustment to the present solar activity is not possible. To gain orbit-averaged fluxes, the user needs to generate the trajectory and provide the model with required coordinates to perform the computation. Fortunately, SPENVIS software is able to execute the transformation automatically [18, 19].

Models CREME-96 and ISO 15390 were engaged in simulations of solar particles and GCR, respectively. The resulting plots are shown in Fig. 2.1 - 2.6. CREME-96 engages phenomenological models in predicting the SEU rates. The model is based on two assumptions - the trail left by the ion is much narrower than the minimum feature size in the affected circuit and that SEU sensitivity in the particular circuit can be assigned to a single sensitive junction. According to authors, since the time of CREME-96 development, the scale of microelectronic components decreased by more than a factor of 100 which is very challenging demand on the model. As well as AP-8 and AE-8 models, despite the obvious need of updated models, they are currently the state-of-the-art tools in SEU simulations.

The energy spectra of electrons and protons trapped in Van Allen belts on the sun-synchronous in the altitude of 530 km are shown in the Fig. 2.1. The most abundant are electrons with energies below 1 MeV reaching the integral flux of $10^6 \text{ cm}^{-2}\text{s}^{-1}$. Compared to electrons of the same energy, protons are approximately thousand times less abundant indicating their fluxes to be in the order of $10^3 \text{ cm}^{-2}\text{s}^{-1}$. With the increasing energy, the flux decreases logarithmically. To test the effects of protons on pixel detectors designed for this mission, particles with energies greater than 1 MeV were chosen. Their abundance in radiation belts is lower; however, consequences of their penetration are more considerable. During the experiments, fluxes of such particles were intentionally chosen much higher than simulated values to get the information about the worst case scenarios.

The space environment considerably varies with respect to the orbit on which the satellite or the spacecraft operates. The choice of the specific orbit depends greatly on the purpose of the mission. Among the most occupied orbits are the Geosynchronous Orbit (GEO), specific case of which is the Geostationary Orbit, the Sun-synchronous Orbit (SSO) and the Low and Middle Earth orbit (LEO, MEO).

LEO, MEO and GEO are characterized by their altitude. This is not the case for SSO which is defined mostly by its inclination. The majority of spacecraft is operating at LEO for its low altitude and thus lower energy requirement to reach it. Remote sensing missions, whose objective is to scan Earth's surface and investigate objects on it, can gain from its relative proximity to Earth to achieve a better resolution. The possible range of altitudes of LEO varies between 100 and 2000 km among sources [22]. Circular GEO is specified by the period of one orbit which is 23 hours, 56 minutes and 4 seconds to match the Earth's rotation. Therefore, the spacecraft is placed to the altitude of 35 786 km above the sea level. The synchronization of the orbit period and the Earth's rotation leads to the fact that from the observer's point of view the spacecraft passes the same point on the surface at the same time of a day. During the following 24 hours it remains at the same longitude moving north or south.

As mentioned above, there is a specific type of GEO - the Geostationary Orbit. This orbit follows the equatorial plane which makes the spacecraft fixed in one position from the observer's point of view. This leads to numerous advantages - antennas do not need to track satellite's movement and the spacecraft is always in view which allows to use them

for example for telecommunication purposes.

The MEO orbit is situated between LEO and GEO. The most common altitude is approximately 20 000 km above the sea level which yields the orbit period of 12 hours. Among the best known missions placed on MEO is the GPS system.

The Sun-synchronous orbit as already stated is not defined by its altitude, although the most commonly used are 900 and 1200 km. The key factor is its inclination which is relatively high - more than 90° . Such an inclination, near to the polar orbit, allows to scan the most of the Earth's surface. However, the main advantage of SSO is the constant illumination by the Sun which is very desirable for example for the solar channels adjustment [22, 23].

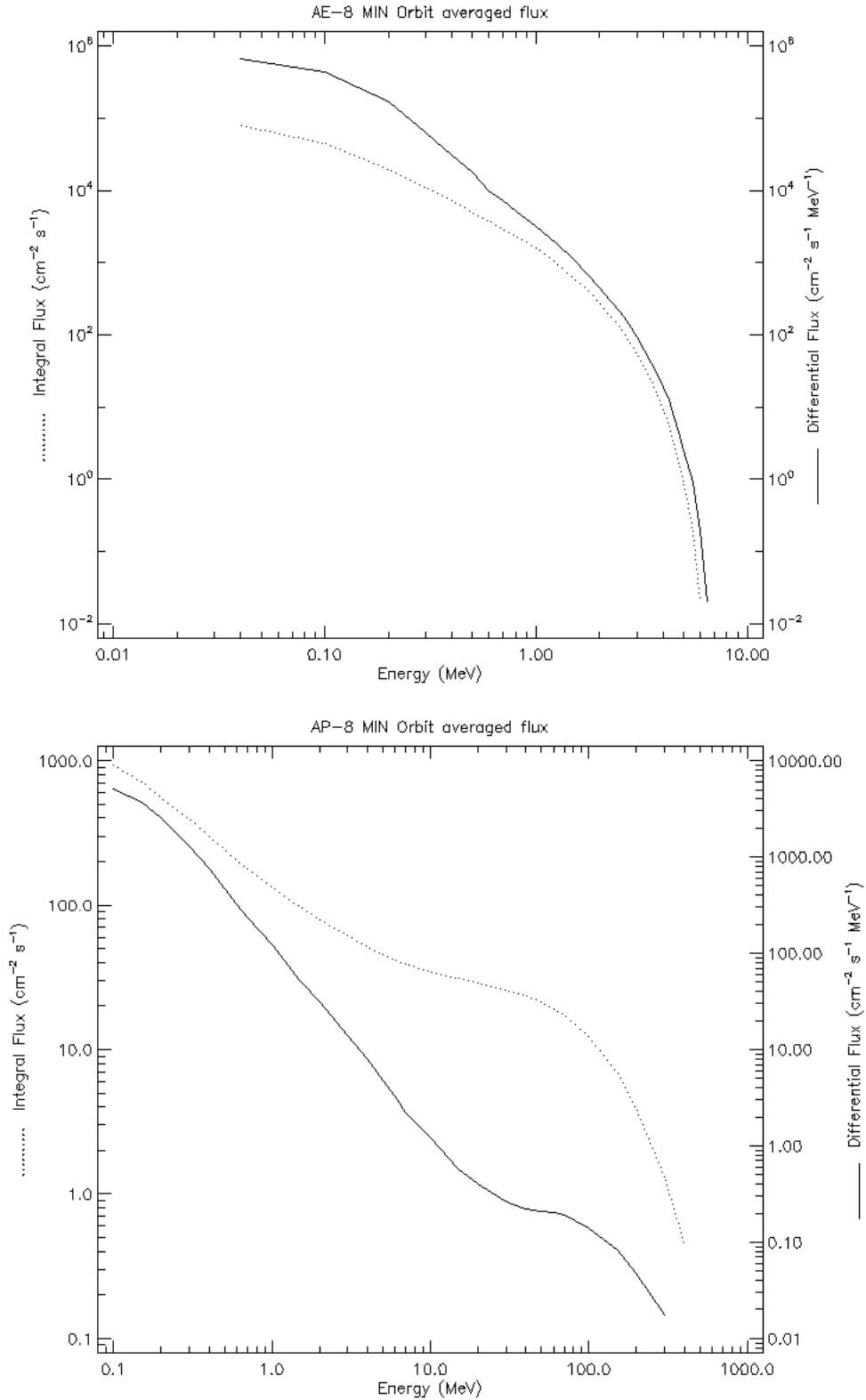


Fig. 2.1. The energy spectra of electrons and protons trapped in Van Allen belts simulated using the SPENVIS software. Both the integral and the differential flux can be seen. The integral flux is the number of particles that cross an unit area per unit of time with the energy greater than the respective value on the x-axis. In order to enumerate the differential flux, the values of energy are normalized to 1 MeV.

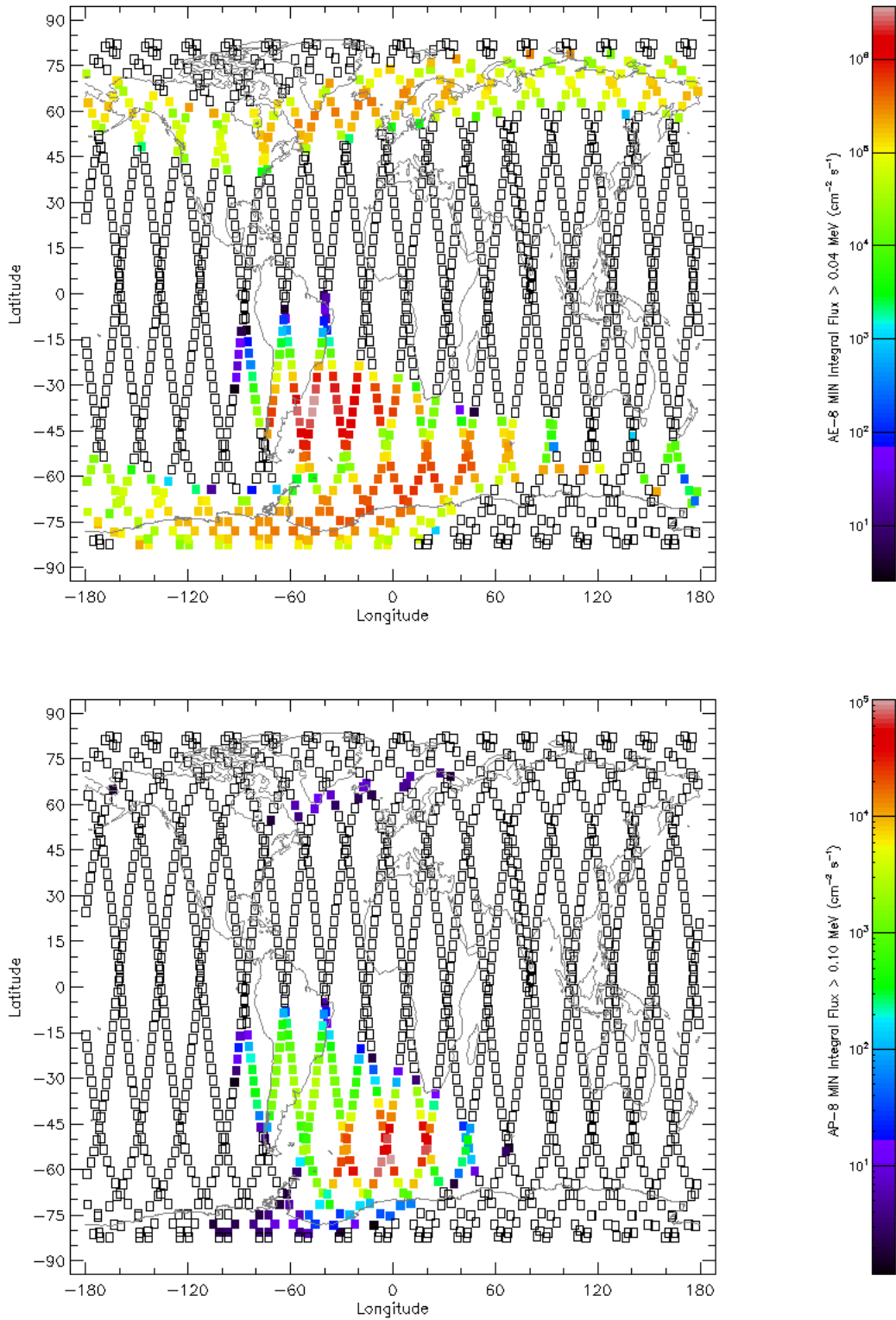


Fig. 2.2. The trajectory of the SOCRAT-R mission on its orbit. The time of one orbit is 95 minutes. Areas of the high electron and proton abundance, simulated using AE-8 and AP-8 models, are clearly visible. From the shape of the Earth's magnetosphere emerges that Van Allen belts penetrate the atmosphere in the region of poles and also South Atlantic Anomaly due to the inclination of the rotational axis of Earth.

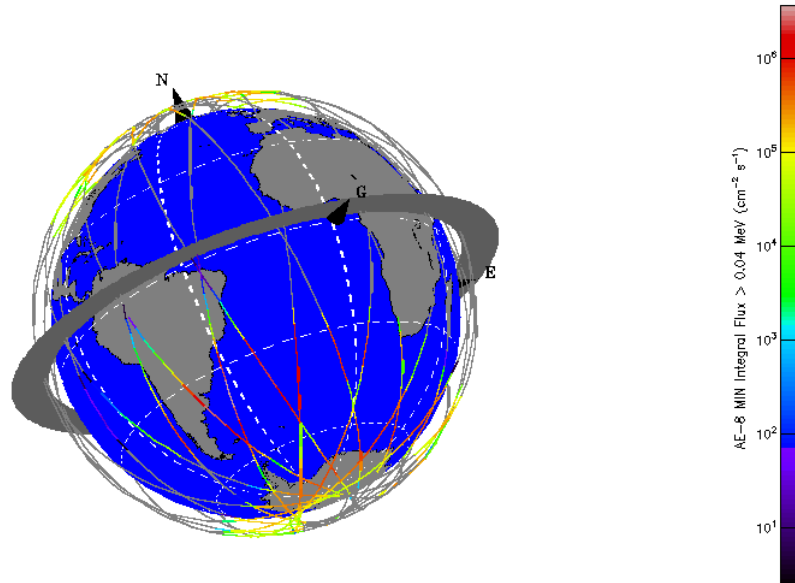


Fig. 2.3. The three-dimensional visualization of the satellite trajectory on its orbit crossing the above described areas of risky abundance of trapped particles which are marked with red in accordance with the present scale. In this case, only electrons are taken into account for the simulation using AE-8 model. The SAA region is clearly visible and can be compared to the schema in Fig. 2.4 [20].

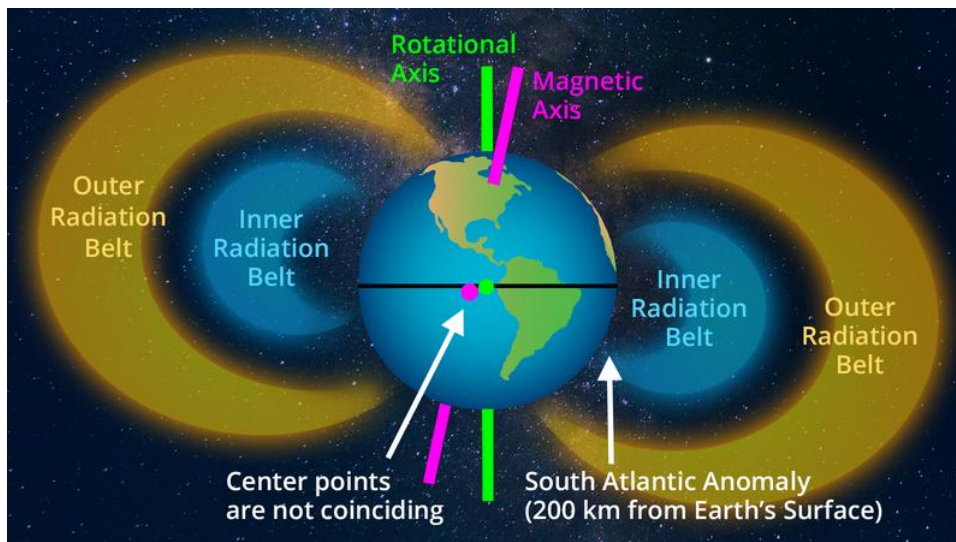


Fig. 2.4. The schema of radiation belts. Because of the deflection of the magnetic axis from the rotational axis, the inner radiation belt is crossing the Earth's atmosphere in the area of the South Atlantic.

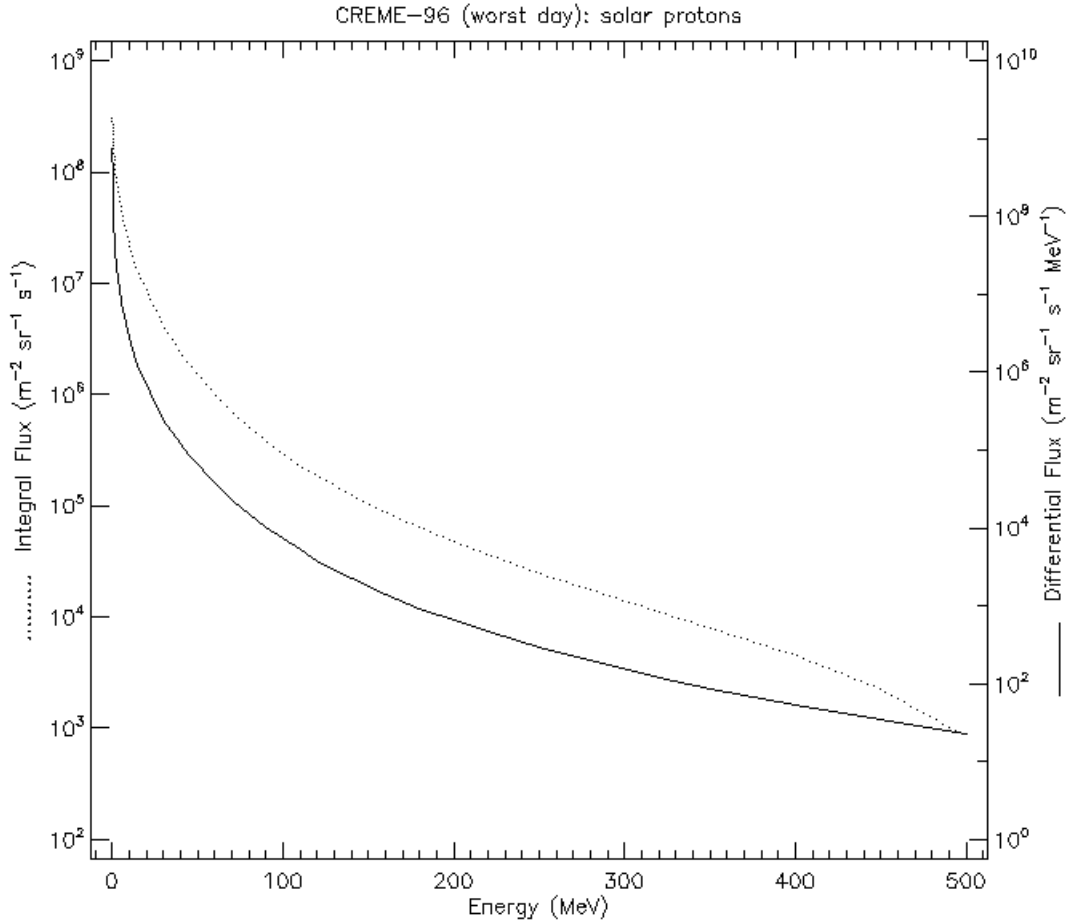


Fig. 2.5. The worst-day simulation of solar protons integral flux using CREME-96 model. Extraordinary solar events can have serious impact not only on devices on orbits but also on systems on the Earth such as radio blackout how was previously explained. The typical example is the solar storm in 1859 known as Carrington Event when auroras were observable all over the world. The solar storm of a similar magnitude occurred in 2012 although it closely missed the Earth. According to NASA report, the storm would presumably cause wide power blackouts [21].

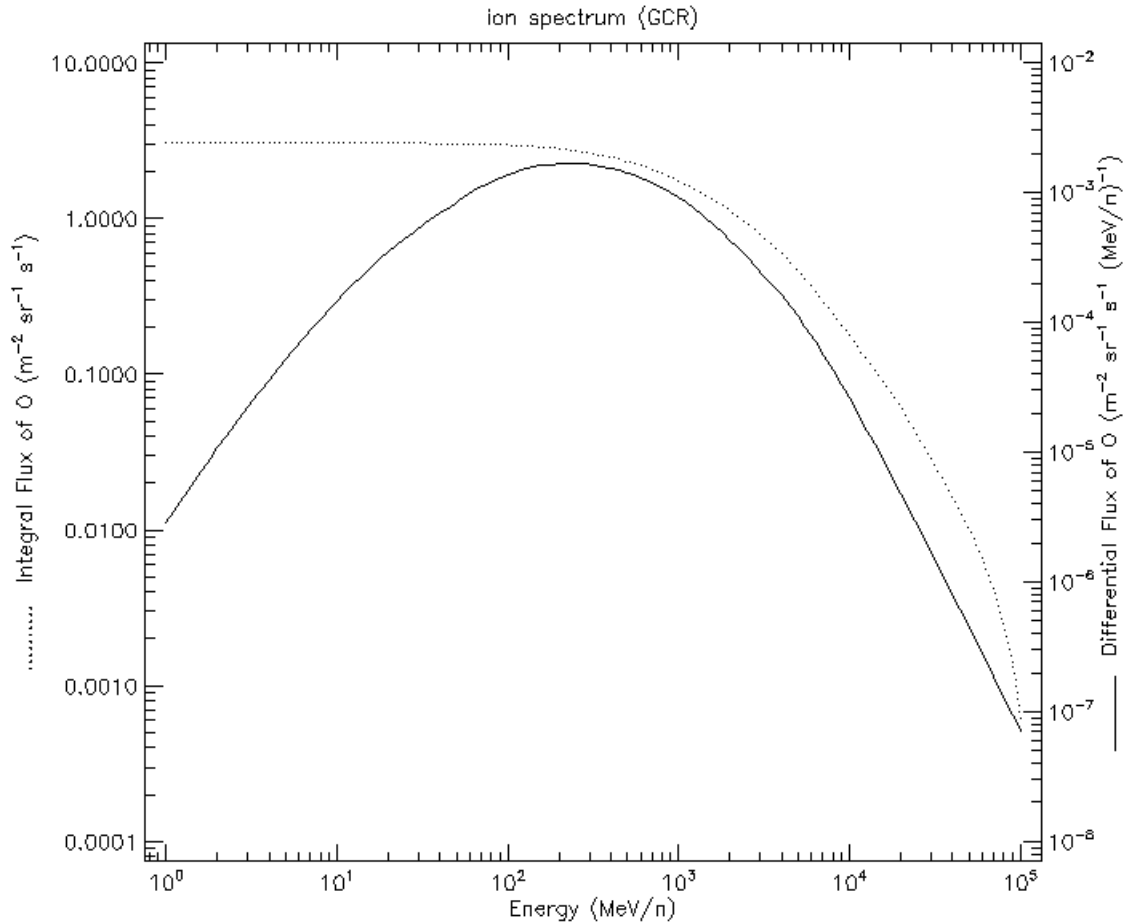


Fig. 2.6. The last main contributor to the overall radiation environment to be discussed are GCRs. For the simulation, oxygen was chosen to match the result with the experiment performed at the Tandetron accelerator, Řež. Fluxes of heavy ions are very low compared to those of protons and electrons. However, effects induced by these ions are an important subject of our investigation because single event upset cross-section is dependent on the particle mass. Although encountering heavy ions is very unlikely, the amount of SEUs induced by them is much higher than the one of the more abundant lighter elements.

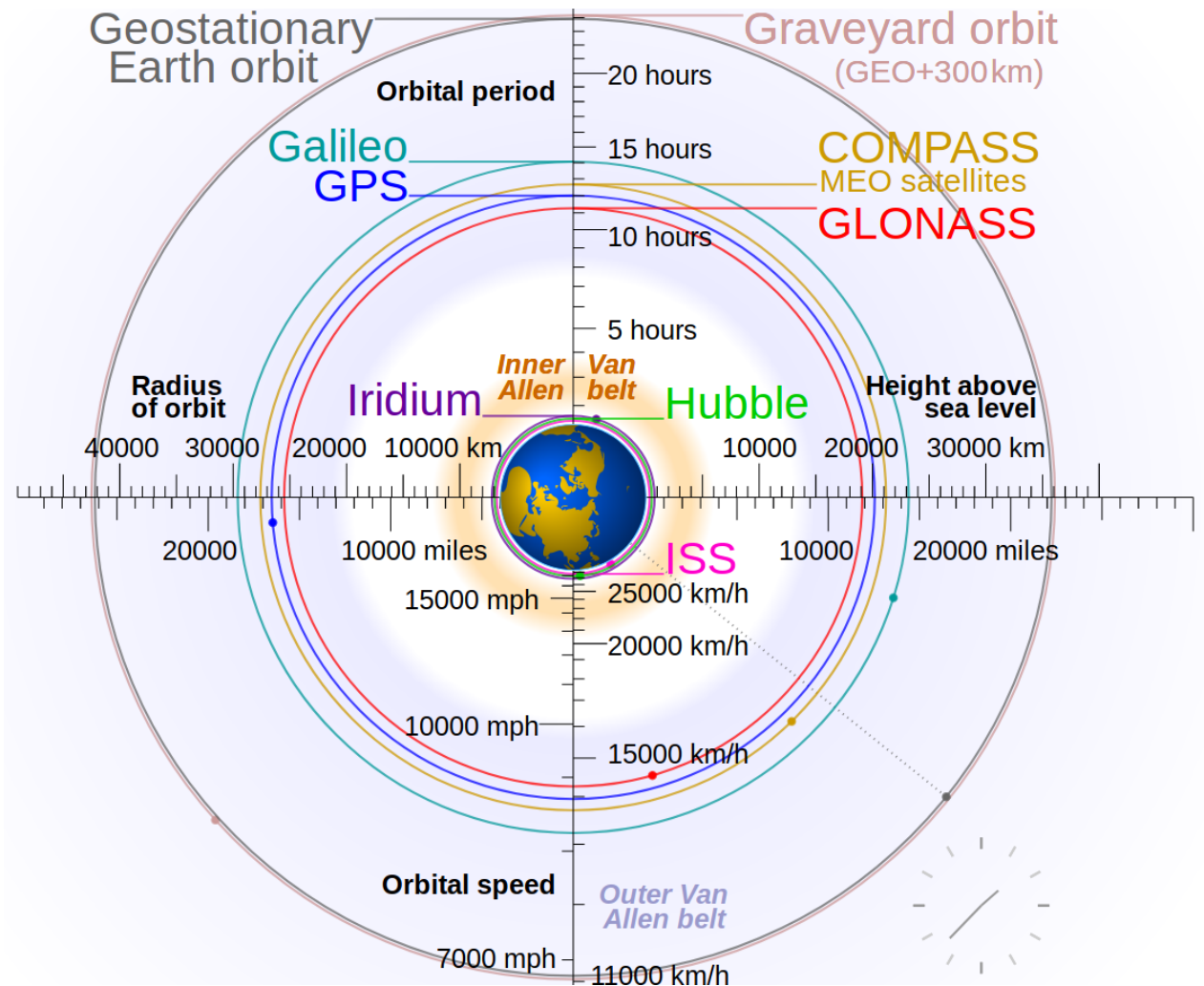


Fig. 2.7. The most occupied orbits of Earth. Altitudes, periods and velocities of different missions can be seen. The inner and outer Van Allen belts are also pictured so that demands on the radiation hardness of the particular spacecraft are put into context [24].

3 Radiation damage in semiconductors

In general, there are several different ways how radiation can impact semiconductor technologies. From the degradation of the material which they are composed of, through the changes in the active components of the circuits, to the failure of the system caused by a single particle passing through it. The process of the improvement of systems that leads to higher radiation tolerance is called *radiation hardening*.

The term *radiation hardening* itself is broad and includes design improvements, a proper shielding or for example error-processing techniques. By combining multiple of these techniques, a sufficient radiation tolerance can be achieved [25].

Depending on the specific application of the designed device, different kinds of particles in wide range of energies can affect it. Photons can interact through three basic processes: the photoelectric effect, the Compton scattering and the electron-positron pair generation. Charged particles are either interacting through the Coulomb forces or undergo nuclear interactions. Neutrons can be elastically or inelastically scattered or cause transmutation reactions. What process is taking place in the given moment depends on the energy of the primary particle. Understanding these interactions is the prerequisite for the proper radiation-tolerant design. However, the situation can be simplified to the most general case - charged particles lose the dominant amount of their energy by ionization processes and neutrons through scattering. This implies the primary division of effects in the semiconductors to those resulting from ionization and those from displacement damage. Naturally, both degradation types can be also caused by different kind of particles with lower probability [25].

In semiconductors, the ionization process starts with the charged particle interacting with the valence electron in the material. As a result of the interaction, the electron is excited to the conduction band. The excess kinetic energy of this electron and the respective hole is then quickly lost by the lattice scattering in the process of *thermalization*. The electron-hole pair is then separated by the energy of the band gap of the involved material. Subsequently, a small fraction of pairs undergoes recombination as the vast majority is free to drift through the material. As a result of the charge movement, parasitic currents occur and can have either temporary (SEU) or permanent consequences (single event latch-up - SEL). The charge carriers can also get trapped in the defect site creating internal space-charge fields and cause shifts in the device characteristics. This can also happen in insulators, like SiO_2 , even though the mobility of electron-hole pairs is much smaller. [25].

So called *total-dose ionization effects* are caused by the previously described mechanism of charge trapping which is especially significant in the vicinity of insulating layers

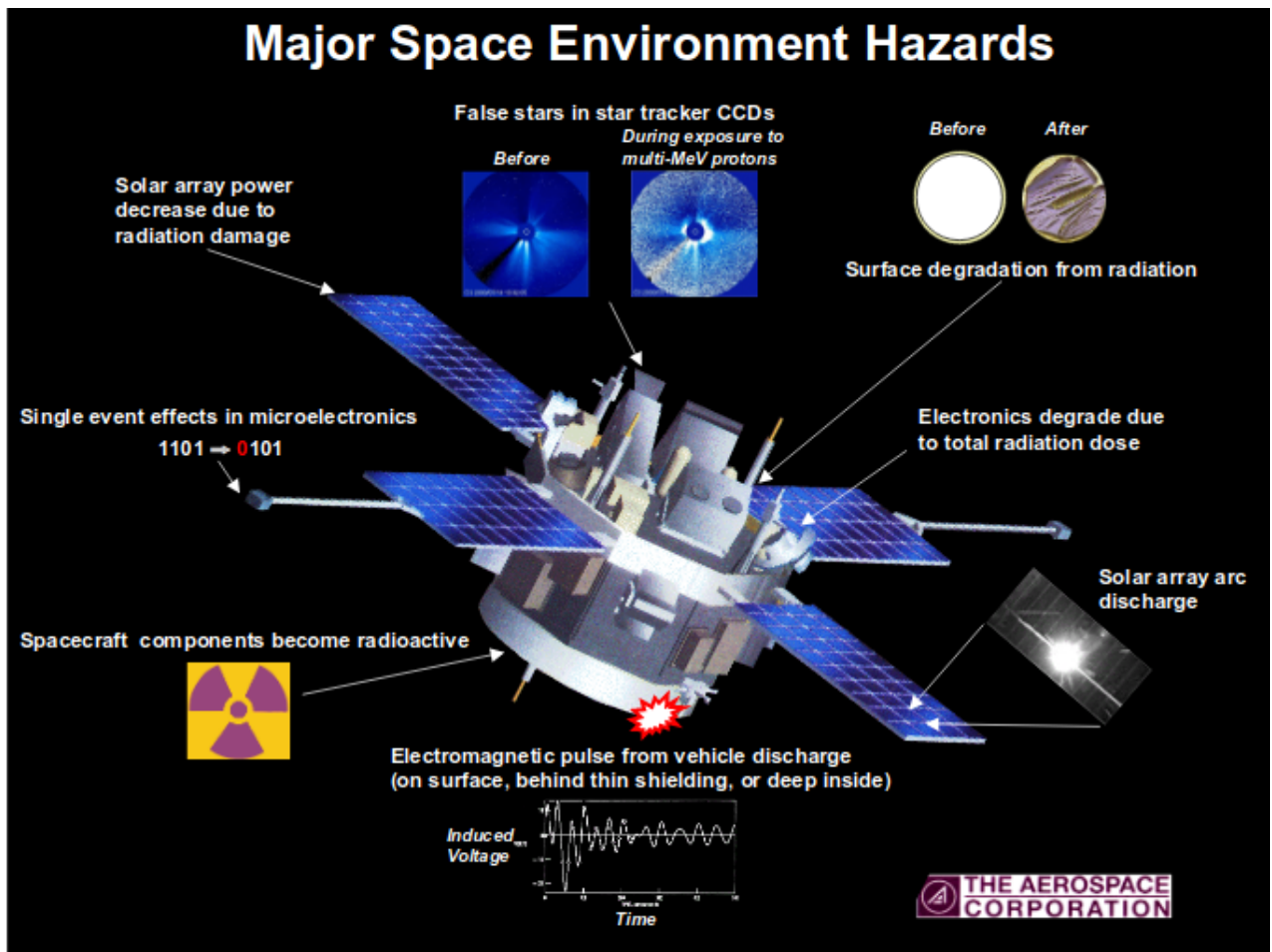


Fig. 3.1. Different types of space-environment-induced effects on a spacecraft [26].

in the device.

The displacement damage is induced by a particle with a sufficient energy in the non-ionizing process during which an atom of the crystalline lattice is dislocated from its current position. As long as the energy of both is above certain threshold, they proceed through the lattice site displacing more atoms from it until they stop. Vacancies, interstitials and sometimes defect clusters are created in the material. These defect sites produce new energy levels in the forbidden band which cause the alternation of properties of the device [25].

The Fig. 3.1 shows several of the discussed malfunctions directly assigned to specific parts of the spacecraft.

4 Radiation tolerance of X-CHIP-03

As described in the previous chapter, there are several ways how the penetrating particle can negatively influence electric devices. Since the X-CHIP-03 is (among other purposes) the cosmic radiation detector prototype, it needs to prove certain qualities of radiation hardness so that the lifetime of the device is sufficient in the harsh environment of the Earth's orbit. For this reason, several experiments testing its capabilities were performed.

4.1 Simulations of experiments

Before running the actual accelerator experiment, a detailed simulation of the passage of different types of charged particles through every layer of the detection system should be done. In order to test particular device properties, it is required that the charged particle reaches the relevant part of the system. The specific type of particle interaction with the material of the detector is dependent on its energy. The selection of the initial energy is crucial because heavy charged particles transfer most of their energy at the end of their range. The curve describing this behaviour is called the *Bragg curve* and the region of the greatest energy deposition *Bragg peak*. During the preparation of an experiment it is important to investigate the ideal initial energy of used charged particles so that the Bragg peak will be placed in the chosen region of the detector. Several kinds of software, among which there are e.g. Geant4 or SRIM, serve this purpose.

Specifically, in the case of the X-CHIP-03 testing, the area of interest was the top 14 μm of the chip where the shift registers sensitive to SEE are placed.

However, sometimes it is useful to aim for the region even deeper in the chip that is actually detecting the used ions, so that a visual check of particle penetration is provided. From simulation, information about the amount of deposited energy in the area and the particle range can be gained.

4.1.1 Geant4

Geant4 is a software set of tools dedicated to Monte Carlo simulation of passage of particles through matter [27]. Besides high energy physics, it is used in astrophysics, radiation protection or medicine. With the aid of this software, a very precise geometry of the simulated detector can be designed, including specific materials which it is made of. If the required material is not available in the author-provided package, it can be defined by the user from individual elements with the knowledge of their ratio in the material [28].

The user is also invited to define physical processes that will be included in the simulation. Trying to reduce the computation time as much as possible, sometimes it is not necessary to simulate all of the possible interactions that a real particle undergoes but are irrelevant

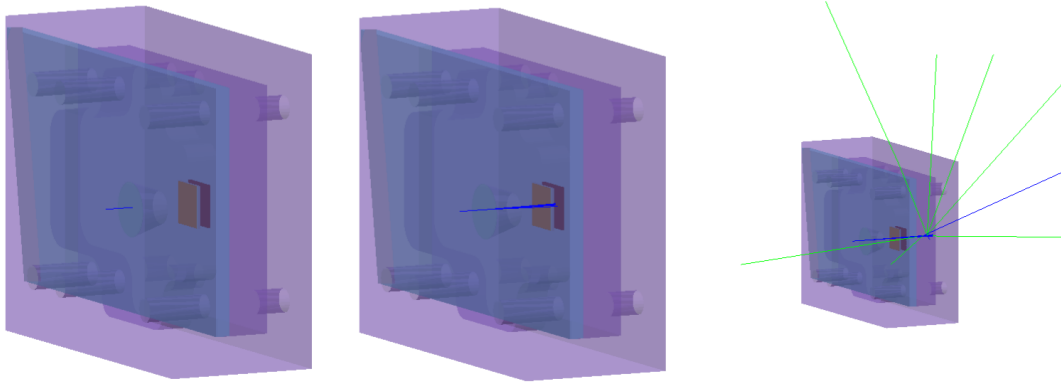


Fig. 4.1. The simulation of the penetration of the prototype of SpacePix Radiation Monitor by α particles of energies 2, 50 and 100 MeV respectively.

for the investigated situation. The user therefore chooses either from defined packages of interactions or creates one themselves, similarly to the definition of materials.

Particles can originate from a point source, isotropically from all directions or from a source with user-defined geometry. Geant4 also allows to track the trajectories of secondary particles created by the passage of the primary particle through the detector which it generates regularly after a defined step.

Another advantage of the software is the possibility of visualisation and control through the user interface [28].

An example of a simple Geant4 simulation is in Fig. 4.1. The pictured detector is named SpacePix Radiation Monitor (SXR) and is composed from several SpacePix chips which are successors of tested X-CHIP-03. The simulation shows the result of the penetration of SXR by α particles of different energies. It can be seen that particles with the lowest energy (2 MeV) have fully stopped right after the collision in the thin titanium shielding placed on the window of the detection system. Particles with energy of 50 MeV cross several layers and are stopped in the volume of the detector. However, particles with the highest simulated energies, on the other hand, are able to pass through the detector while creating secondary particles which are marked with the green color.

■ 4.1.2 SRIM

SRIM [29] is a software dedicated to a simulation of passage and range of particles with the energy up to 2 GeV/amu through matter. Similarly to Geant4, it provides a great amount of applications such as calculation of the energy loss and range of the particle, simulation of the ion implantation used for the modification of the irradiated sample or the effects of the hadron therapy on the oncology patients. In comparison with Geant4 it is much older - the first version was developed already in 1983.

First, the user defines the individual layers of the detector according to the ratio of chemical elements, subsequently they choose the width of each layer. The next step is to select the ions for irradiation and their energy. After the simulation is run, it is possible to plot a number of graphs directly in the interface including the spatial distribution of

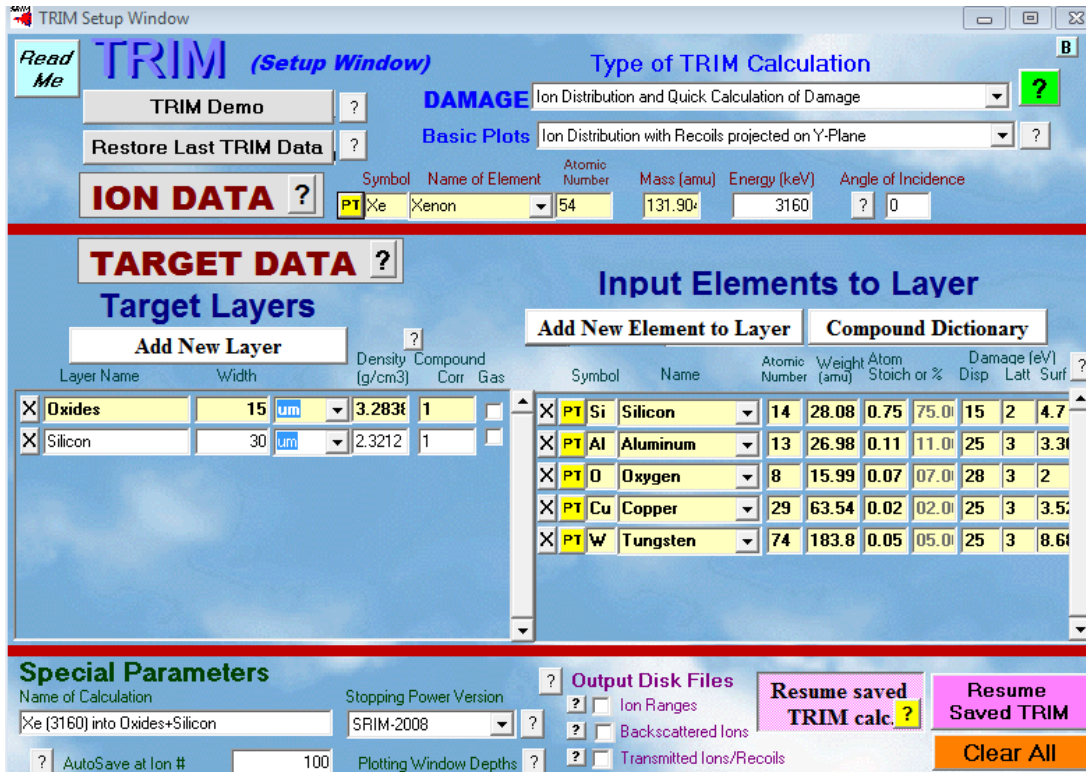


Fig. 4.2. The user interface of SRIM software for the detector formation and the selection of ions.

ions which is the most important one from the experiment preparation point of view. The individual stages of the simulations are shown in Fig. 4.2 - 4.4.

From the last picture it can be derived that the greatest amount of the deposited energy is located in the sensitive part of the chip. For this reason, simulated energies were used in the real-life experiment.

4.2 Single event upset evaluation

One of the important characteristics of the X-CHIP-03 is the exact irradiation level affecting in particular single event upsets (SEUs) - bit flips. The bit flip is an alternation in binary information in digital part of detection chip. During previous experiment run at the tandem accelerator Tandetron in Nuclear Physics Institute of the Czech Academy of Sciences, Řež, integral fluence 10^{12} ions/mm² of proton, helium and carbon was reached and no significant effect was observed. Therefore, the next step was to use ions with higher linear energy transfer (LET).

4.2.1 Experiment in Joint Institute for Nuclear Research

In Joint Institute for Nuclear Research (JINR) in Dubna, Russia, experiment was run at the accelerator complex U400M. U400M is an isochronous cyclotron that started operating in 1991 and specializes in acceleration of *radioactive beams*, very neutron-rich and thus radioactive elements.

In the Table 4.1, ions used for irradiation, their LET and integral fluence reached during



Fig. 4.3. The process of simulation in SRIM software.

Ion	Energy [MeV/n]	Fluence [10^6 cm^{-2}]	#Bit-flips
$^{22}\text{Ne}^{10+}$	3,33	157 ± 53	3085
$^{40}\text{Ar}^{16+}$	3,48	234 ± 67	7442
$^{136}\text{Xe}^{46+}$	3,16	$92,1 \pm 27,7$	2387

Tab. 4.1. Parameters of ions used for the SEU tolerance test in JINR.

irradiation can be found.

Ions with sufficient energy can reach the sensitive area of the chip and create clusters, as is shown in Fig. 4.5.

4.2.2 Experiment in the Nuclear Physics Institute

On Tandetron, a tandem accelerator located at the Nuclear Physics Institute of Czech Academy of Sciences, Řež, Czech Republic, X-CHIP-03 was irradiated by ions with lower LET than in Dubna - namely carbon and oxygen. X-CHIP-03 was placed in a vacuum chamber. Table 4.2 summarizes parameters of used ions. Their energies emerge from Monte Carlo simulations run in Geant4 as mentioned above, as well as SRIM simulations provided by NPI CAS. A visualisation of these simulations can be seen in Fig. 4.6.

The most recent irradiation was performed in August 2019 and was focused on protons alone. The aim was proving the theory that the investigated technology is highly tolerant to protons with energy of several MeVs that reliably penetrate the insensitive layers of the chip to the sensitive area. The reached fluence was as high as 10^{12} particles per cm^2 . No SEUs were observed during this experiment providing us the evidence, that all the possible proton-induced malfunctions can be caused only by nuclear reactions, not ionization process.

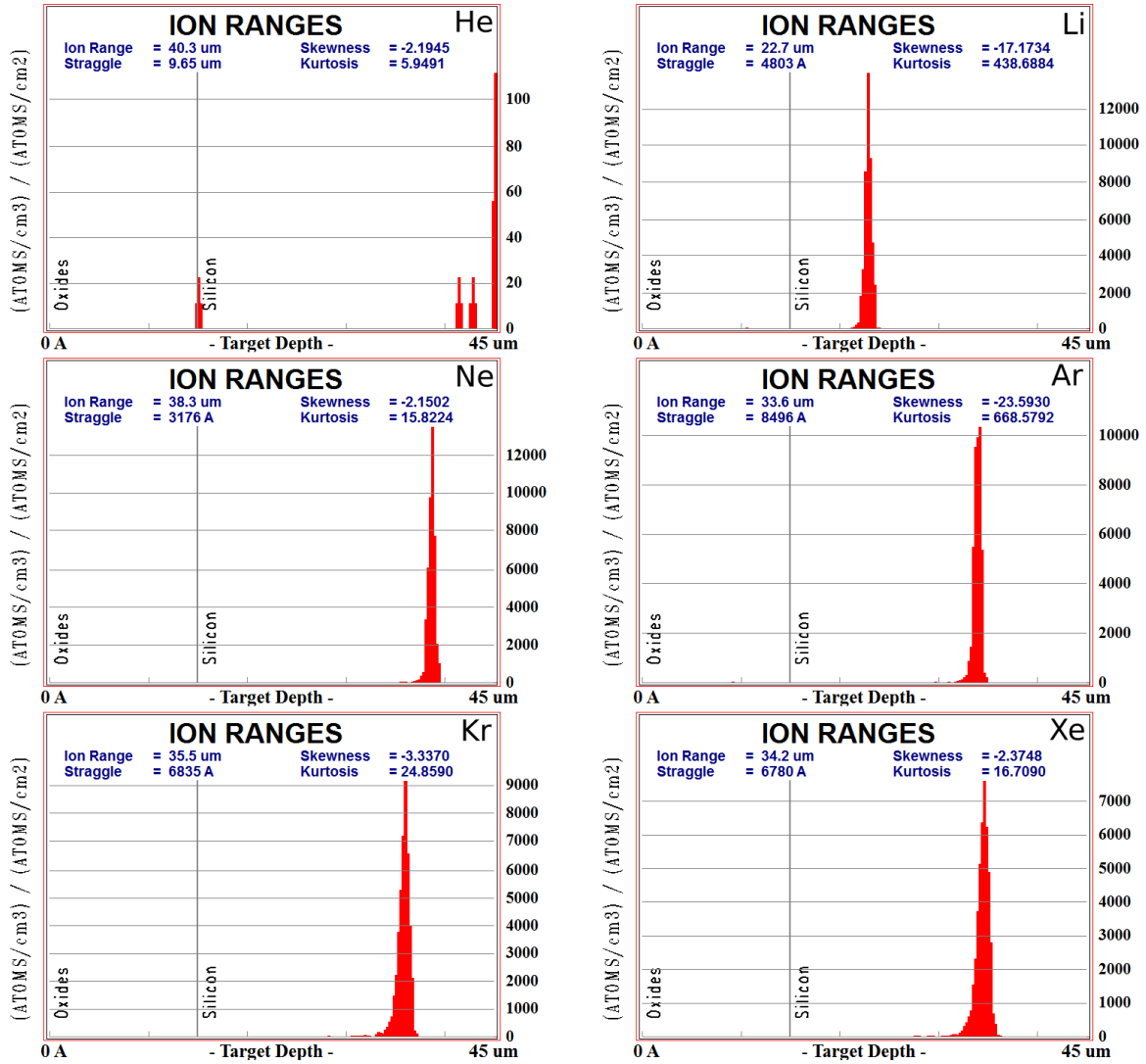


Fig. 4.4. Plots in SRIM software showing the range of ions in the designed detector which is pictured in the longitudinal cross-section. Individual layers are marked and labelled.

Ion	Energy [MeV/n]	Fluence [10^{10} cm^{-2}]	#Bit flips
C	17	9	0
C	17	3,5	3
C	17	30	43
C	17	12	52

Tab. 4.2. Parameters of ions used for a SEE tolerance test at the NPI CAS.

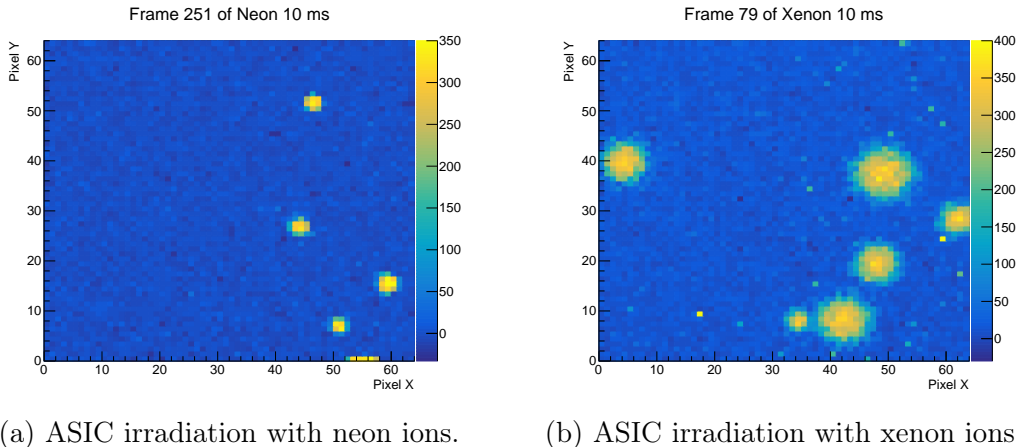


Fig. 4.5. Individual frames taken during irradiation by (a) neon ions and (b) xenon ions forming clusters.

The placement of X-CHIP-03 in the vacuum chamber in NPI CAS, in JINR respectively, can be found in Fig. 4.8 and Fig. 4.7.

4.2.3 Results

Based on the data collected during the experiments at JINR and NPI CAS, LET dependence of SEU cross-section was evaluated. The calculation of cross-section σ_{SEU} is performed as follows [30]

$$\sigma_{SEU} = \frac{N_{SEU}}{K\phi}, \quad (4.1)$$

where N_{SEU} is the number of observed SEUs (in this particular case the number of bit-flips), ϕ is the integral flux of particles used for the irradiation and K is the number of bits of the circuit where can SEU occur (in our case 1024 bits).

The resulting curve is shown in Fig. 4.9. The desired radiation tolerance was not reached because of a specific component, D flip-flops, which compose the shift registers of the ASIC. This crucial area will therefore be the subject of radiation hardening. However, it is important to state that fluxes used during the experiments exceeded the true cosmic environment values by orders of magnitude.

4.2.4 Homogeneity of bit-flip sensitivity

One important feature of SEU evaluation is the homogeneity of number of occurred bit-flips with respect to its position. In another words, among the 64 columns of the X-CHIP-03, the number of bit-flips in their bytes should be approximately constant. As is shown in Fig. 4.10, this requirement is fulfilled for each column and even among individual bytes. Also, the nature of bit-flip was studied and evaluated. The result is demonstrated in the same picture, where it is clearly visible that the number of flips from 0 to 1 is approximately the same as the number of flips from 1 to 0.

The fact that the sensitivity to radiation is homogeneous among registers and their bytes is very positive. Even though their radiation tolerance was not proven sufficient, behaviour of individual registers is the same which can be relied on in the process of their improvement.

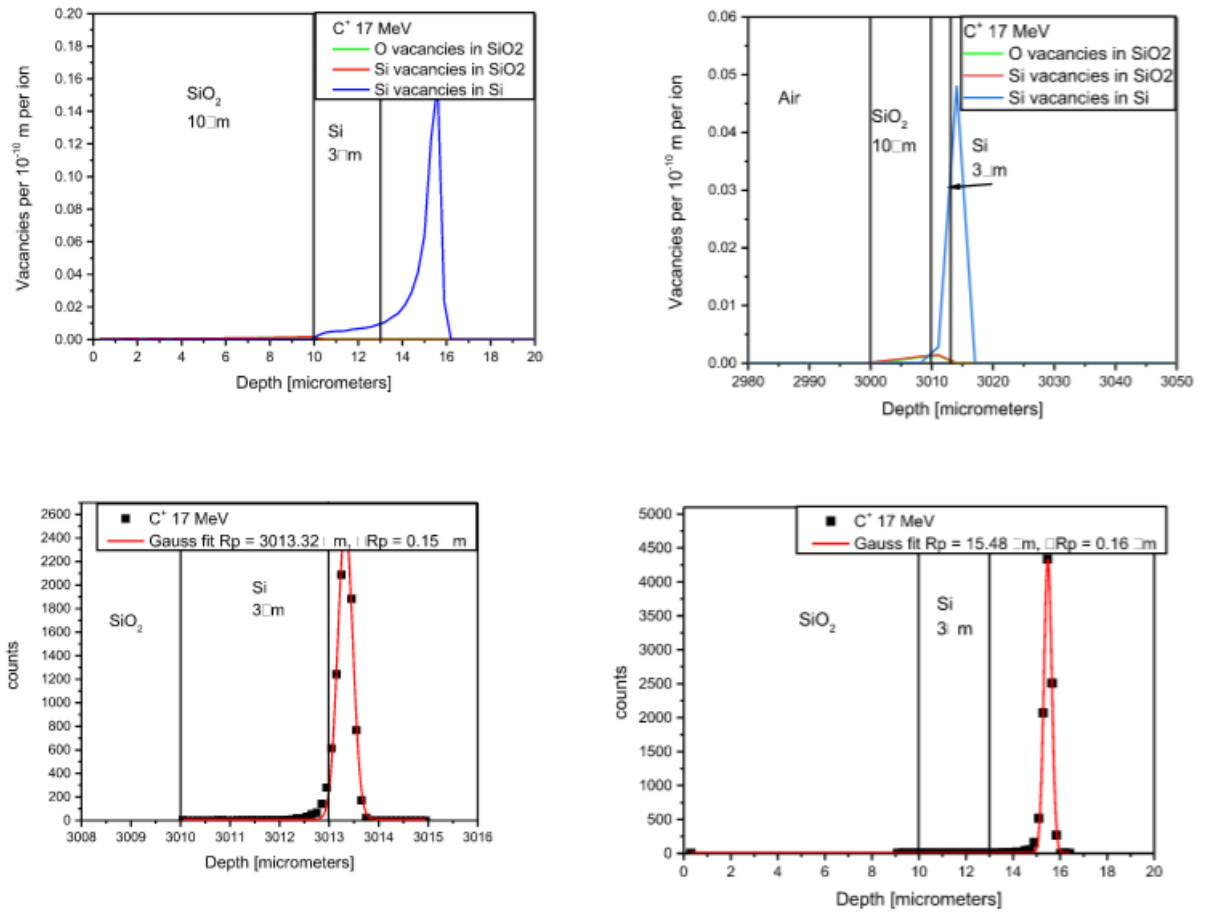


Fig. 4.6. SRIM simulations of deposition of energy of carbon ions passing through X-CHIP-03 volume.

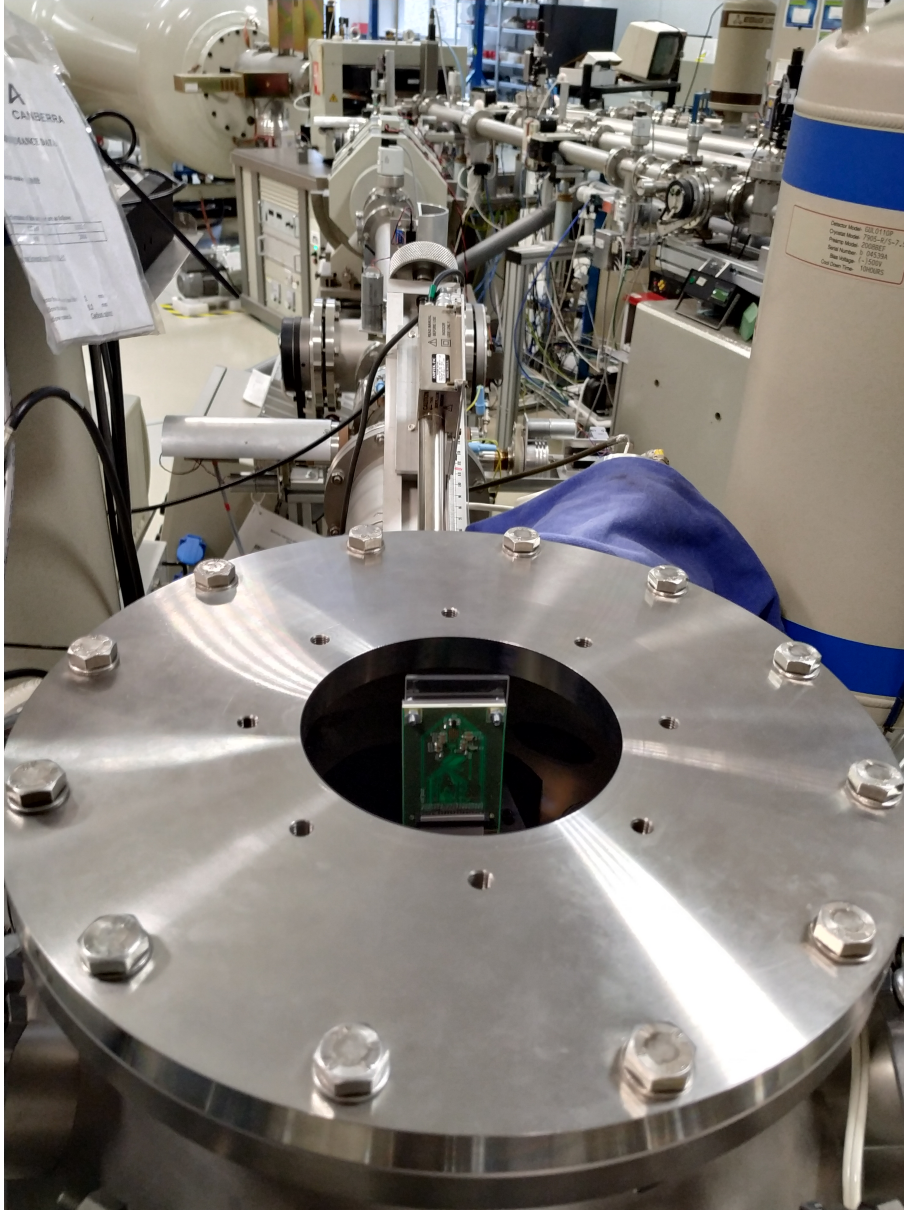


Fig. 4.7. The placement of X-CHIP-03 in the vacuum chamber in NPI CAS on the tandem accelerator Tandetron.

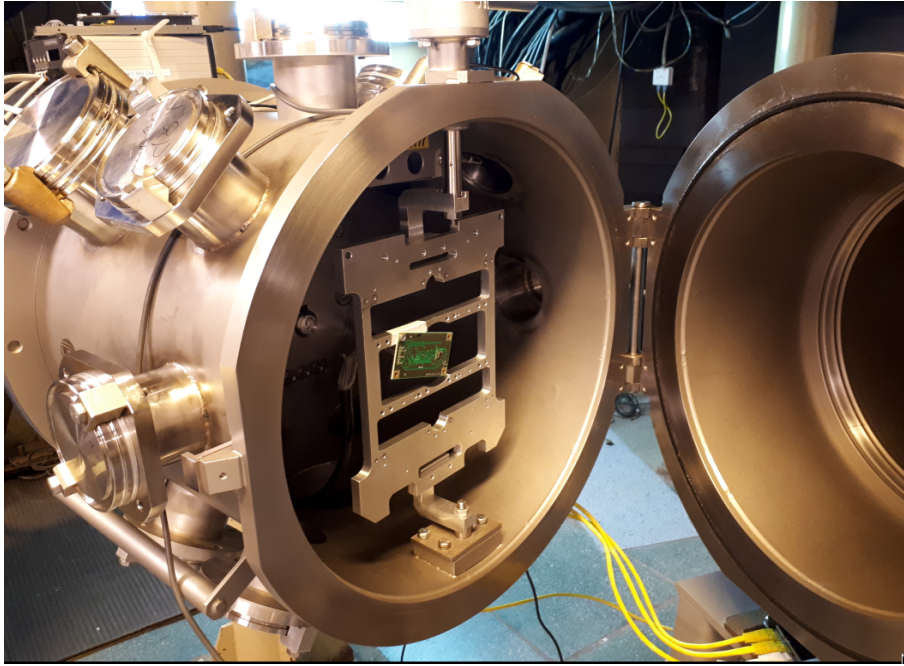


Fig. 4.8. The placement of X-CHIP-03 in the vacuum chamber in JINR cyclotron U400M.

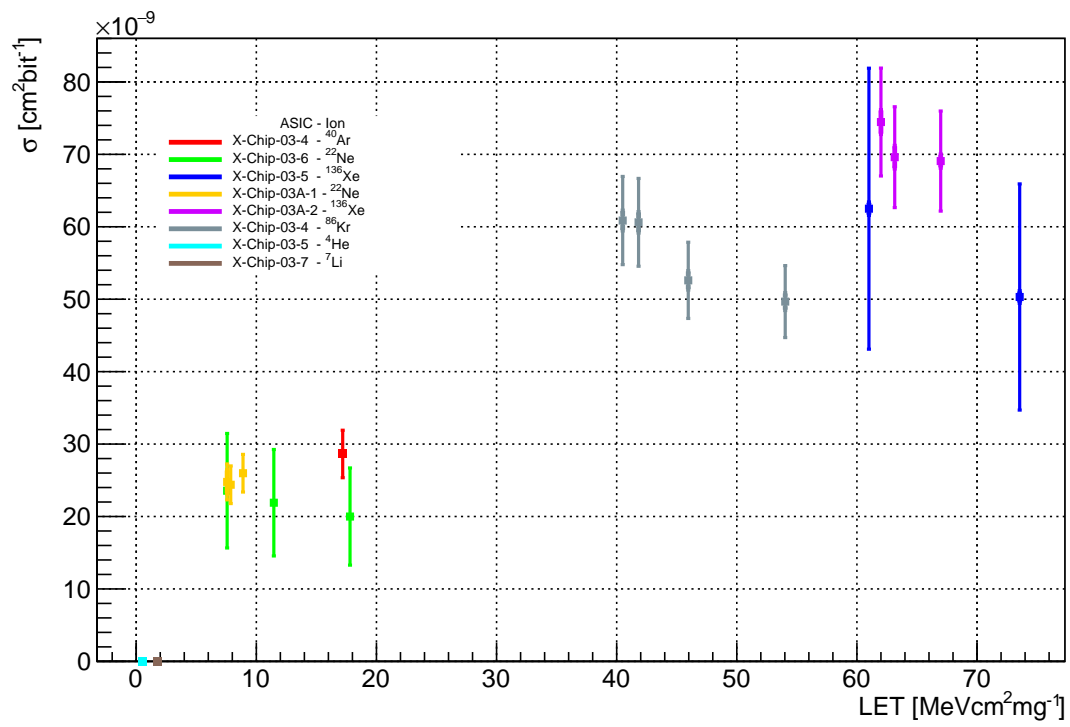


Fig. 4.9. SEU cross-section as a function of LET of ion.

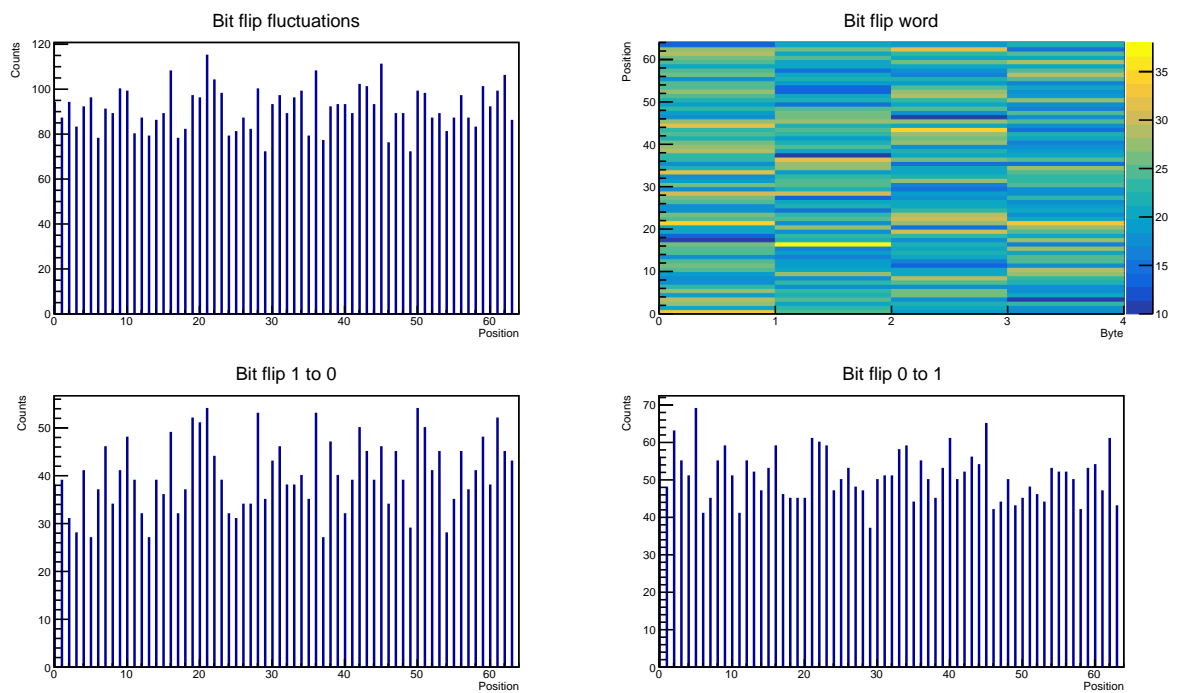


Fig. 4.10. Top left: bit-flip fluctuations with respect to register position. Top right: bit-flip fluctuations among individual bytes. Bottom: number of flips from 1 to 0 (left) and from 0 to 1 (right) with respect to the register position.

5 Characterization of X-CHIP-03 response

So far, only one of the possible applications of X-CHIP-03 was discussed. As a cosmic radiation monitor, X-CHIP-03 should provide the outcome containing the particle identification and its energy while in ADC mode. However, the device can be also used for the spectroscopy. For this purpose, X-CHIP-03 was inserted in the SpacePix Demonstrator that was developed in the Center of Applied Physics and Advanced Detector Systems at the Faculty of Nuclear Sciences and Physical Engineering in cooperation with esc Aerospace. Response of SpacePix Demonstrator to radionuclide sources of ^{55}Fe and ^{238}Pu clearly resolves the main photon energy peaks and the pedestal, as can be seen in the Fig.5.1.

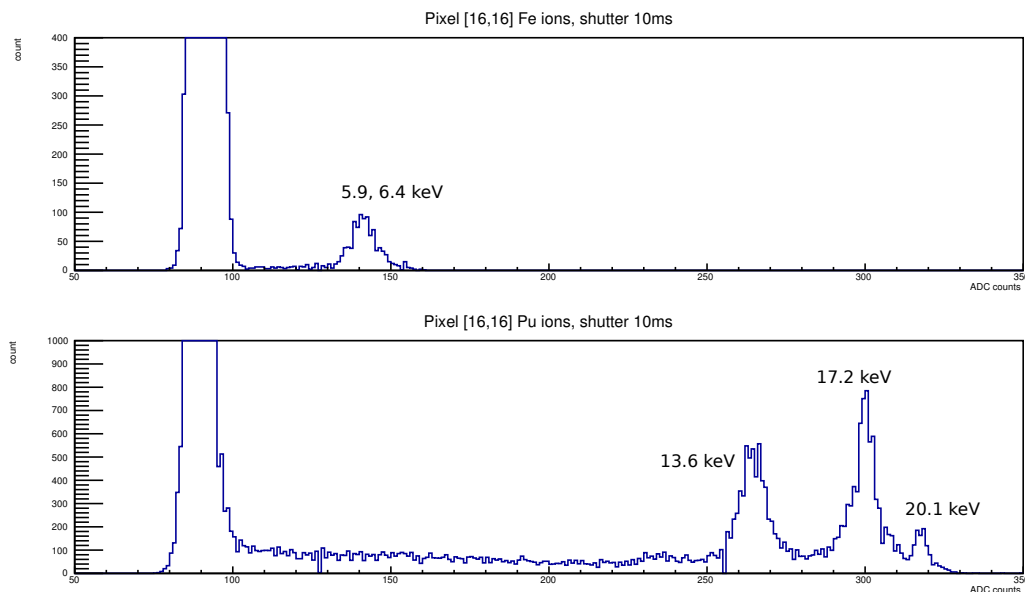


Fig. 5.1. Gamma-spectra of ^{55}Fe and ^{238}Pu evaluated using SpacePix Demonstrator with X-CHIP-03.

An important feature of each detection ASIC is the response at the level of individual peaks. When the penetrating particle leaves some specific amount of energy during its path through volume of the chip, the acquired response is in so called ADC units (units of analogue-digital converter). To get the information about the original energy, each pixel has to be calibrated because during the fabrication, minor differences for each circuit can occur which then result in the slightly different characteristics. Well-known spectra, such as the above mentioned gamma spectra of iron and plutonium, can be used for this

purpose. Each measured peak of certain value in ADC units corresponds to an existing peak of the spectra of known energy. For the calibration, 3 peaks were used: one peak of iron and two peaks of plutonium of values in Table 5.1. The fourth peak of plutonium which is listed in the table and also detected by SpacePix Demonstrator was not taken into account because it is easily mistakable for the background excess. For each value, a pedestal has to be subtracted so the absolute value in ADC units is compared to the known-spectra. The result is the calibration curve that is pixel-specific, as can be seen in Fig. 5.2.

Radionuclide	Peak energy [keV]	Response of pixel [ADC units]
^{55}Fe	6	53
^{238}Pu	13.6	177
^{238}Pu	17.2	217
^{238}Pu	20.1	236

Tab. 5.1. Values of energies of individual peaks in spectra of iron and plutonium and response of one specific pixel in ADC units.

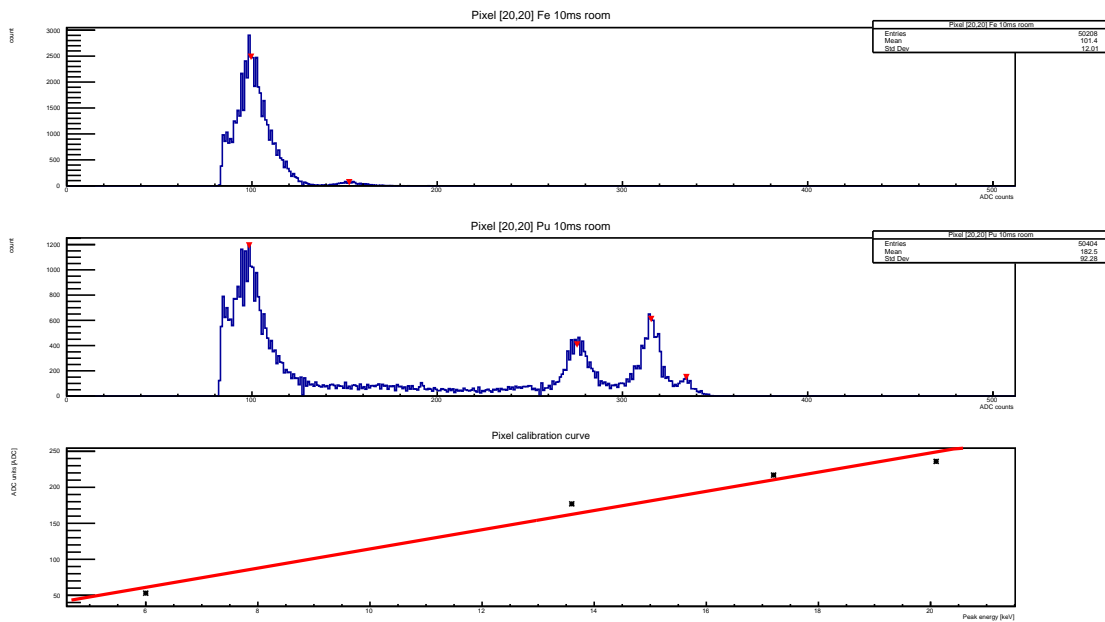


Fig. 5.2. Peaks found (depicted by red arrows in the first two images) in chosen known spectra and calibration curve of pixel (20, 20) of X-CHIP-03.

The important feature of the detecting device is its stability across wide temperature range. Especially in cosmic environment, where temperatures can oscillate considerably more than in laboratory conditions. Two different experiments directed at the response difference resulting from the temperature change were therefore performed. SpacePix demonstrator was used for measurement in -5°C , 20°C and 60°C . The difference in response is the well-known feature and was therefore not surprising. Such behaviour needs to be taken into account in the calibration assuming that information about temperature of the device can be provided. Preliminary results imply that for each temperature, a specific calibration curve will need to be used. The second experiment was not using SpacePix Demonstrator but proto-SXRM. SXRM,

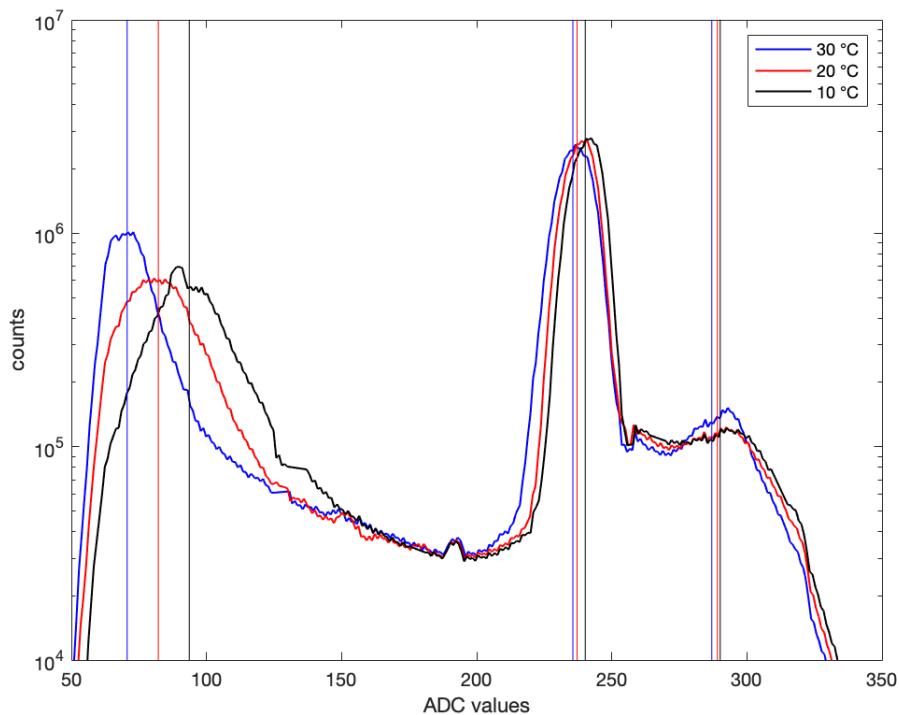


Fig. 5.3. The proto-SXRM response to the plutonium irradiation at different temperatures. The pedestal movement (in the left part of the spectra) is more noticeable than the movement of spectral peak.

or SpacePix Radiation Monitor, is detector composed of multiple layers of SpacePix detecting chips, design of which is based on the X-CHIP-03. Proto-SXRM is a smaller, more compact version of the future SXRM that was used for the first in-situ test during the Socrat-R mission which will be later described in detail. Based on the previous results from SpacePix Demonstrator, the temperature dependence of the response of the device was also expected. The spectra of plutonium was measured in 10°C, 20°C and 30°C. From the resulting plot Fig. 5.3 it is clear that especially the pedestal movement is impacted by the temperature change. Characteristic peaks overlap; however, their absolute value is changing slightly due to the pedestal values. Another noticeable fact is that one peak of plutonium is not properly distinguishable in the spectra. It is challenging to identify the missing peak and therefore assign those present to the corresponding known-values. For this reason, energy calibration could not be performed. However, information gained from this experiment can serve as a reference for the future data from the orbit.

The next step in this part of X-CHIP-03 testing would be the application of the performed calibration on the old and new data and proving that it does not contain any major mistakes. Also, calibration can be adjusted to other devices. For that, it needs to be more universal which would be the future subject of my work.

6 X-CHIP-03 in space

The future goal of the Center of Applied Physics and Advanced Detector Systems (CAPADS) is to develop a very light and compact radiation monitor for the wide usage all over the Earth's magnetosphere to provide a complex picture of its characteristics. As explained before, the harsh environment is the main constraint of space exploration, especially concerning manned missions possibly reaching for the Moon or Mars.

The summary of the Socrat-R mission, where CAPADS contributed with the cosmic environment monitor proto-SXRM, follows. This is the first mission where the future family of radiation monitors has been tested in-situ providing the group a unique feedback of its capabilities and also information about the space weather.

The proto-SXRM is composed of two X-CHIP-03 layers. The design of the future device SXRM, that is already prepared and currently being simulated, counts with five-layer arrangement. For this mission, the proof of concept engaging two layers was prepared.

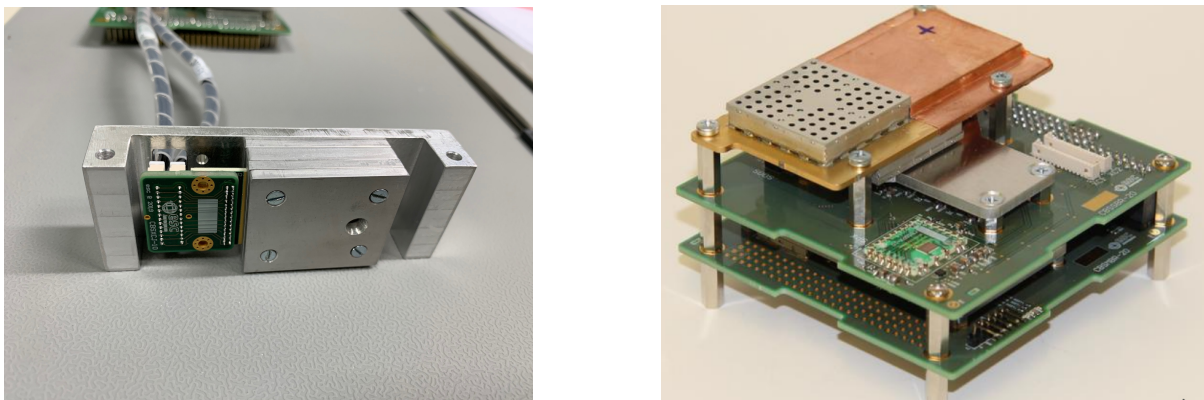


Fig. 6.1. Left: The proto-SXRM detector placed in the supporting frame. The chip is located in the conical hole in the middle of the top aluminium layer. In the hole, the titanium shielding is placed to improve the radiation hardness of the device and to extend its lifetime. Right: The complete module composed of several Czech experiments, among them proto-SXRM and SpacePix.

The proto-SXRM, primarily dedicated to detection of protons and electrons, is placed in the module accompanied by other Czech contributions - the SpacePix detecting chip for the detection of protons and heavy ions, the unique PC104 platform ESCOBC for the data processing and reduction equipped with radiation-tolerant memory cells, and SpaceDos dosimeter for cosmic rays detection. This is the result of cooperation of multiple academic groups - CAPADS at Faculty of Nuclear Sciences and Physical Engineering of the Czech Technical University in Prague, the Nuclear Physics Institute of the Czech Academy of Sciences and esc Aerospace which is also responsible for the fabrication of

the module in Fig. 6.1.

The module is placed on the nano-satellite Socrat-R based on the standardized CubeSat platform manufactured at the Lomonosov Moscow State University. Together with other CubeSats, it has been inserted into the deployer (Fig. 6.2) responsible for its launch while reaching the orbit. All of the CubeSat missions were launched before the satellite Meteor M2-2 reaches its goal orbit approximately 300 km higher.



Fig. 6.2. Left: Three CubeSats ready for the launch. The first from right is containing the Czech module. Right: The deployer that is responsible for the ejection of the CubeSat once it is on the sun synchronous orbit.

The carrier rocket was a three-stage Soyuz-2.1b/Fregat (Fig. 6.4). The launch took place at Vostochny Cosmodrome on 5th July 2019. After the problem-free launch, the deployer ejected Socrat-R on its goal orbit 530 km above the sea level. The mission is currently in the commissioning phase - its functionality is being tested. If successful, detectors are going to be turned on and ready to use. This unique inspection of the low orbit radiation environment will be the main subject of my future activity in the CAPADS group.



Fig. 6.3. The detail of the mission arrangement. The dominating part equipped with the solar panel is weather satellite Meteor M2-2. On the left, deployers with CubeSats are mounted.



Fig. 6.4. The Soyuz-2.1/Fregat three-stage rocket before launch on 5th July 2019 at the Vostochny Cosmodrome.

7 Conclusions

This research task was aiming for the compact description of the cosmic environment monitoring mission from its beginning - the simulation of the radiation fluxes in the particular orbit, through the rigorous testing of the instrumentation, to the end - the launch of the rocket that has taken the device on the orbit.

From the first chapter, it is clear that the near-Earth space environment is a very complex and intricate region. Being influenced and formed by various sources, energy of particles ranges from keVs to hundreds of MeVs. The flux of the particles is highly dependent on the certain orbit. For this reason, the Spensiv software was used for multiple simulations showing the flux of protons and electrons trapped in Van Allen belts formed by the Earth's magnetosphere, the flux of solar protons during the solar cycle minimum, and the flux of oxygen representing the contribution of galactic cosmic rays containing heavy ions. The reader was also introduced to different types of orbits most frequently used for current space missions of all purposes.

Once the environment was described, the chapter dedicated to the radiation damage in semiconductors followed. A very brief overview of basic interaction processes was offered for better understanding of two general radiation induced damage mechanisms - ionization and displacement damage. Included in the former, single event upsets were introduced. Single event upset, malfunctions caused by a single particle penetrating the device, were the objective of the further work.

The device for high-energy particle detection needs to prove a certain level of radiation hardness to be able to operate in harsh conditions they give rise to. Especially the X-CHIP-03, a prototype of future cosmic radiation detecting chip, needs to demonstrate a sufficient radiation tolerance and provide the feedback of its functionality so potential changes can be incorporated to future designs. The experimental part of this paper starts with the description of simulations performed. For each planned experiment, a simulation needs to be provided, for the right beam energy adjustment. Geant4 and SRIM, two software tools that serve this purpose, were presented. SRIM was engaged in the subsequent preparation of one of the following experiments that took place at the Nuclear Physics Institute of the Czech Academy of Sciences using the Tandatron accelerator. The summary of the experiments follows. Besides the above mentioned, another set of experiments was performed in the Joint Institute for Nuclear Research in Dubna, Russia. The device was irradiated by many various ions and protons and the SEU cross-section was established as a result. Besides that, details of occurred errors distribution in the digital part of the device were analysed.

The next chapter contains the characterization of the device response, specifically the relationship between the natural units of X-CHIP-03 circuits (so-called ADC units) and the true value of the energy of the detected particle. Also, the response was monitored for different temperatures within two separate and independent sets of experiments.

The highlight of the paper is the description of the mission launch accompanied with pictures of components of the experiment with commentary provided.

The further steps are certainly the analysis of data taken on the orbit that should be available any day, the generalization of the performed calibration on other similar devices that could be universally implemented and improvements of the cosmic radiation detectors designs.

Literature

- [1] M. Havranek et al. X-chip-03: Soi maps radiation sensor with hit-counting and adc mode. *2018 IEEE Nuclear Science Symposium and Medical Imaging Conference Proceedings (NSS/MIC)*, pages 1–4, Nov 2018.
- [2] V. A. Skuratov et al. Roscosmos facilities for see testing at u400m flnr jinr cyclotron. *2011 12th European Conference on Radiation and Its Effects on Components and Systems*, pages 756–759, Sep. 2011.
- [3] A. Mackova et al. A. Romanenko. Performance and application of heavy ion nuclear microbeam facility at the nuclear physics institute in Rež, czech republic. *Review of Scientific Instruments*, 90:013701, 01 2019.
- [4] V. Vrba et al. The SpacePix-d radiation monitor technology demonstrator. *Journal of Instrumentation*, 13(12):C12017–C12017, dec 2018.
- [5] Stuff in Space. <http://stuffin.space/?intlides=2019-038AE&search=socra>.
- [6] S. Clark. Soyuz rocket and fregat upper stage deliver 33 satellites to three different orbits. *Space Flight Now*, 2019.
- [7] Space Weather Prediction Center. Galactic cosmic rays. <https://www.swpc.noaa.gov/phenomena/galactic-cosmic-rays>.
- [8] M. Andre Ch. Macdonald. Strategies and geant4 simulations for radiation protection on an eml-2 mission. 06 2015.
- [9] Space Weather Prediction Center. Solar flares and radio blackouts. <https://www.swpc.noaa.gov/phenomena/solar-flares-radio-blackouts>.
- [10] Space Weather Prediction Center. Radiation belts. <https://www.swpc.noaa.gov/phenomena/radiation-belts>.
- [11] D. P. Stern. The magnetopause. <https://www-spof.gsfc.nasa.gov/Education/wmpause.html>.
- [12] D. Steel. *Rogue Asteroids and Doomsday Comets: The Search for the Million Megaton Menace That Threatens Life on Earth*. Wiley, September 1997.
- [13] D. Koschny. About the near-earth object coordination centre. https://m.esa.int/Our_Activities/Space_Safety/About_the_Near-Earth_Object_Coordination_Centre.
- [14] Space Sciences. Space environment, nature of the. *Encyclopedia.com*.
- [15] ESA. Space safety: The story so far. http://www.esa.int/Our_Activities/Space_Safety/The_story_so_far.
- [16] ESA Belgian Institute for Space Astronomy. Spenvis. <https://www.spenvis.oma.be/>.
- [17] J. Lauenstein and J. L. Barth. Radiation belt modeling for spacecraft design: model comparisons for common orbits. *IEEE Radiation Effects Data Workshop, 2005.*, pages 102–109, July 2005.

-
- [18] J. I. Vette. The ae-8 trapped electron model environment. *NSSDC WDC-A-RS Report 91-24*, 1991.
- [19] J. I. Vette D.M. Sawyer. Ap-8 trapped proton environment for solar maximum and solar minimum. *NSSDC WDC-A-RS 76-06*, 1976.
- [20] A. Hamer. The south atlantic anomaly is the bermuda triangle of space. <https://curiosity.com/topics/the-south-atlantic-anomaly-is-the-bermuda-triangle-of-space-curiosity/>.
- [21] T. Phillips. Near miss, the solar superstorm of july 2012. https://science.nasa.gov/science-news/science-at-nasa/2014/23jul_superstorm/.
- [22] Global Change Master Directory. Ancillary description writer's guide. <http://gcmd.nasa.gov/User/suppguide/>.
- [23] National Research Council. *Orbital Debris: A Technical Assessment*. The National Academies Press, Washington, DC, 1995.
- [24] L. Bonenberg. Closely-coupled integration of locata and gps for engineering applications. 01 2014.
- [25] F. B. McLean and T. R. Oldham. Basic mechanisms of radiation effects in electronic materials and devices. 9 1987.
- [26] J. E. Mazur. Space environment effects on space systems. https://www.lpi.usra.edu/meetings/LEA/presentations/wed_am/1_Mazur_Space_Weather_Impacts.pdf.
- [27] J. Allison et al. Geant4 developments and applications. *IEEE Transactions on Nuclear Science*, 53(1):270–278, Feb 2006.
- [28] S. Agostinelli et al. Geant4—a simulation toolkit. *Nuclear Instruments and Methods in Physics Research Section A: Accelerators, Spectrometers, Detectors and Associated Equipment*, 2003.
- [29] J. F. Ziegler, M. D. Ziegler, and J. P. Biersack. Srim - the stopping and range of ions in matter (2010). *Nuclear Instruments and Methods in Physics Research B*, 268:1818–1823, jun 2010.
- [30] F. Zhang et al. Y. Wang, Ho. Guo. Sram single event upset calculation and test using protons in the secondary beam in the bepc. *Journal of Semiconductors*, 32(9):092001, sep 2011.

List of figures

- 1.1 Experimental set of SpacePix Demonstrator and currently used ASIC - X-CHIP-03. 1
- 1.2 Left: The orbit of the Socrat satellite carrying the detection device X-CHIP-03 [5]. Right: The start of Soyuz rocket carrying the Socrat satellite from the Vostochny Cosmodrome in eastern Russia [6]. 2
- 2.1 The energy spectra of electrons and protons trapped in Van Allen belts simulated using the SPENVIS software. Both the integral and the differential flux can be seen. The integral flux is the number of particles that cross an unit area per unit of time with the energy greater than the respective value on the x-axis. In order to enumerate the differential flux, the values of energy are normalized to 1 MeV. 8
- 2.2 The trajectory of the SOCRAT-R mission on its orbit. The time of one orbit is 95 minutes. Areas of the high electron and proton abundance, simulated using AE-8 and AP-8 models, are clearly visible. From the shape of the Earth’s magnetosphere emerges that Van Allen belts penetrate the atmosphere in the region of poles and also South Atlantic Anomaly due to the inclination of the rotational axis of Earth. 9
- 2.3 The three-dimensional visualization of the satellite trajectory on its orbit crossing the above described areas of risky abundance of trapped particles which are marked with red in accordance with the present scale. In this case, only electrons are taken into account for the simulation using AE-8 model. The SAA region is clearly visible and can be compared to the schema in Fig. 2.4 [20]. 10
- 2.4 The schema of radiation belts. Because of the deflection of the magnetic axis from the rotational axis, the inner radiation belt is crossing the Earth’s atmosphere in the area of the South Atlantic. 10
- 2.5 The worst-day simulation of solar protons integral flux using CREME-96 model. Extraordinary solar events can have serious impact not only on devices on orbits but also on systems on the Earth such as radio blackout how was previously explained. The typical example is the solar storm in 1859 known as Carrington Event when auroras were observable all over the world. The solar storm of a similar magnitude occurred in 2012 although it closely missed the Earth. According to NASA report, the storm would presumably cause wide power blackouts [21]. 11

2.6	The last main contributor to the overall radiation environment to be discussed are GCRs. For the simulation, oxygen was chosen to match the result with the experiment performed at the Tandetron accelerator, Řež. Fluxes of heavy ions are very low compared to those of protons and electrons. However, effects induced by these ions are an important subject of our investigation because single event upset cross-section is dependent on the particle mass. Although encountering heavy ions is very unlikely, the amount of SEUs induced by them is much higher than the one of the more abundant lighter elements.	12
2.7	The most occupied orbits of Earth. Altitudes, periods and velocities of different missions can be seen. The inner and outer Van Allen belts are also pictured so that demands on the radiation hardness of the particular spacecraft are put into context [24].	13
3.1	Different types of space-environment-induced effects on a spacecraft [26]. .	15
4.1	The simulation of the penetration of the prototype of SpacePix Radiation Monitor by α particles of energies 2, 50 and 100 MeV respectively.	17
4.2	The user interface of SRIM software for the detector formation and the selection of ions.	18
4.3	The process of simulation in SRIM software.	19
4.4	Plots in SRIM software showing the range of ions in the designed detector which is pictured in the longitudinal cross-section. Individual layers are marked and labelled.	20
4.5	Individual frames taken during irradiation by (a) neon ions and (b) xenon ions forming clusters.	21
4.6	SRIM simulations of deposition of energy of carbon ions passing through X-CHIP-03 volume.	22
4.7	The placement of X-CHIP-03 in the vacuum chamber in NPI CAS on the tandem accelerator Tandetron.	23
4.8	The placement of X-CHIP-03 in the vacuum chamber in JINR cyclotron U400M.	24
4.9	SEU cross-section as a function of LET of ion.	24
4.10	Top left: bit-flip fluctuations with respect to register position. Top right: bit-flip fluctuations among individual bytes. Bottom: number of flips from 1 to 0 (left) and from 0 to 1 (right) with respect to the register position. .	25
5.1	Gamma-spectra of ^{55}Fe and ^{238}Pu evaluated using SpacePix Demonstrator with X-CHIP-03.	26
5.2	Peaks found (depicted by red arrows in the first two images) in chosen known spectra and calibration curve of pixel (20, 20) of X-CHIP-03.	27
5.3	The proto-SXRM response to the plutonium irradiation at different temperatures. The pedestal movement (in the left part of the spectra) is more noticeable than the movement of spectral peak.	28

6.1	Left: The proto-SXRM detector placed in the supporting frame. The chip is located in the conical hole in the middle of the top aluminium layer. In the hole, the titanium shielding is placed to improve the radiation hardness of the device and to extend its lifetime. Right: The complete module composed of several Czech experiments, among them proto-SXRM and SpacePix.	29
6.2	Left: Three CubeSats ready for the launch. The first from right is containing the Czech module. Right: The deployer that is responsible for the ejection of the CubeSat once it is on the sun synchronous orbit.	30
6.3	The detail of the mission arrangement. The dominating part equipped with the solar panel is weather satellite Meteor M2-2. On the left, deployers with CubeSats are mounted.	31
6.4	The Soyuz-2.1/Fregat three-stage rocket before launch on 5th July 2019 at the Vostochny Cosmodrome.	32

List of tables

- 4.1 Parameters of ions used for the SEU tolerance test in JINR. 19
- 4.2 Parameters of ions used for a SEE tolerance test at the NPI CAS. 20

- 5.1 Values of energies of individual peaks in spectra of iron and plutonium and response of one specific pixel in ADC units. 27